Phase extraction pattern recognition

Tuvia Kotzer, Joseph Rosen, and Joseph Shamir

Phase extraction pattern recognition is a special case of nonlinear matched filtering. The phase extraction procedure is executed on the input function's Fourier transform as well as on the filter function's Fourier transform, both of which are manipulated for correlation purposes. This novel process is examined theoretically, by computer simulations and laboratory experiments. The implementation of a coherent electro-optical phase extraction pattern recognition system demonstrates the advantages of this new approach.

I. Introduction

Since the development of the VanderLugt optical correlator[1] various improvements have been suggested, both in terms of the filters employed and in system architecture. Each technique provides its relative advantages and drawbacks, depending on the specific task to be performed.

Today it is relatively well accepted that most of the information about an object lies in the phase of the spatial spectrum of the object and that the amplitude distribution is of subsidiary importance.[2] Hence, respectable efforts have been made in the generation of phase-only filters[3] (POF). The POF may be viewed as the result of a nonlinear (NL) operation performed on some of the information in order to amplify some concealed details. This operation is usually accompanied by the suppression or rejection of some relevant information. For example, higher spatial frequencies are amplified but the information hidden in the amplitude distribution is lost.

The above approach manipulated only the information contained in the reference object that is used to generate the filter for a linear optical correlator. In more recent work some attempts have been made to process jointly the information of the reference together with the input information.[4,7] In particular, Ersoy *et al.*[5,6] introduced the idea of NL matched filtering and, specifically, phase extraction pattern recognition.

This paper deals with the underlying concept of the latter approach that is based on symmetric processing. We perform correlations for pattern recognition purposes by manipulating, solely, the phases of the spectral distributions of the input and filter functions. This work has some relation to the binary joint transform correlator[7–10] (JTC), although in the latter no pure phase extraction is implemented.[8] The binary JTC is also much more sensitive to noise because of the particular thresholding procedure used.[8]

The fundamental principle of this system architecture is similar operations on the information that produces the filter and the actual input distribution during operation. The mathematical background is given in Section 2 while the ideal system performance is investigated by computer simulations in Section 4. A laboratory setup is presented in Section 5 and experimental results, demonstrating the superior performance of this novel system, are described in Section 6. The efficiency of the system is examined in Section 7 while architectural modifications of the original setup are presented in Section 8. Finally, conclusions are presented in Section 9.

II. Basic Considerations

The theoretical implementation of the phase extraction correlator, as presented by Ersoy *et al.*,[5,6] is shown as a block diagram in Fig. 1. The input complex amplitude distribution, $q(x, y)$, is Fourier transformed (FT) and operated on by a point nonlinearity, N_l. The NL operation on a general function,

$$R(u, v) = |R(u, v)| \exp[j\varphi(u, v)],$$

is defined by

$$N_l[R(u, v)] = |R(u, v)|^l \exp[j\varphi(u, v)]; \quad 0 \le l \le 1. \tag{1}$$

The authors are with the Department of Electrical Engineering, Technion–Israel Institute of Technology, Haifa 32000, Israel.

Received 12 February 1991.
0003-6935/92/081126-12$05.00/0.

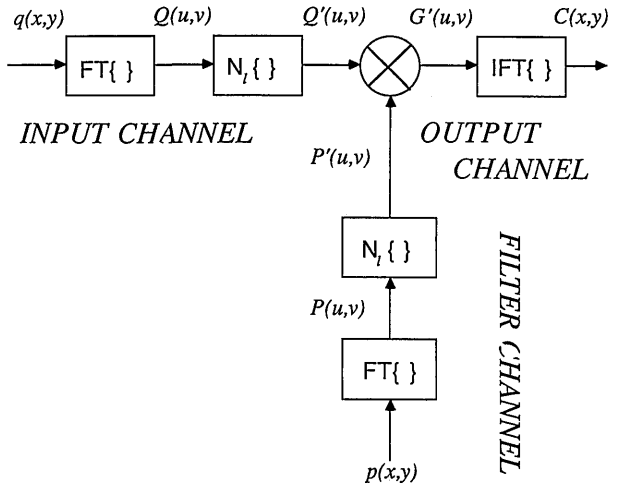

Fig. 1. Block diagram of the symmetric NL correlation: FT and IFT denote the Fourier transform and its inverse, respectively; $q(x, y)$ and $p(x, y)$ are the input and filter functions; N_l is a point nonlinearity.

This paper concentrates on $l = 0$, which means that we extract the phase function from $R(u, v)$. The filter function, $p(x, y)$, undergoes a transformation identical to the input function. The two results are multiplied and the product, $G'(u, v)$, is inverse Fourier transformed (IFT) to yield the correlation output $C(x, y)$. Since this correlator extracts the phase of the input signal as well as of the filter function, we call it a phase extraction correlator. We propose to implement the FT and IFT optically by lenses, while the nonlinearity is performed by digital computer.

When the FT operation is performed on $q(x, y)$ we have

$$Q(u, v) = \mathcal{F}\{q(x, y)\} = A_0 \int\int q(x, y)\exp[-j2\pi(ux + vy)]\mathrm{d}x\mathrm{d}y, \quad (2)$$

where A_0 is a constant, $u = x_f/\lambda f$, $v = y_f/\lambda f$, λ is the light wavelength, f is the focal length of the FT lens, and (x, y) and (x_f, y_f) are the spatial coordinates and spatial frequency coordinates, respectively.

When the NL operation is applied to Eq. (2), with $l = 0$, it yields

$$Q'(u, v) = \exp[j\varphi_Q(u, v)]. \quad (3)$$

In a similar way we have the FT of the filter function,

$$P(u, v) = \mathcal{F}\{p(x, y)\}, \quad (4)$$

and the phase extraction operation,

$$P'(u, v) = N_{l=0}\{P(u, v)\}, \quad (5)$$

which is in fact the conventional POF. When multiplying $Q'(u, v)$ by $P'(u, v)$ we obtain

$$G'(u, v) = Q'(u, v)P'(u, v), \quad (6)$$

and when performing an IFT, at the correlation plane, we obtain

$$C(x, y) = \mathcal{F}^{-1}\{G'(u, v)\} = \int\int \exp[j\varphi_Q(u, v)]\exp[j\varphi_P(u, v)]\exp[j2\pi(ux + vy)]\mathrm{d}u\mathrm{d}v. \quad (7)$$

Some interesting characteristics of the process are investigated with the help of some specific cases.

(a) Single object in the input plane,

$$q(x, y) = a(x + x_0, y + y_0), \quad (8)$$

to which the POF is matched:

$$p(x, y) = a(-x, -y). \quad (9)$$

Substitution of Eqs. (8) and (9) into Eqs. (2), (3), and (7) yields

$$C(x, y) = \delta(x + x_0, y + y_0). \quad (10)$$

This kind of response is identical to that of a theoretical inverse filter that is not constrained by practical limitations.[11]

(b) Two identical objects in the input plane to which the POF is matched:

$$q(x, y) = a(x + x_0, y + y_0) + a(x + x_1, y + y_1), \quad (11)$$

$$p(x, y) = a(-x, -y). \quad (12)$$

Defining

$$\mathcal{F}\{a(x, y)\} = A(u, v) = |A(u, v)|\exp[j\phi(u, v)] \quad (13)$$

and substituting into the proper equations yield

$$Q(u, v) = |A(u, v)|\exp[j\phi(u, v)] \times \{\exp[-j2\pi(ux_0 + vy_0)] + \exp[-j2\pi(ux_1 + vy_1)]\}. \quad (14)$$

By letting

$$2x_2 = x_0 - x_1, \quad 2y_2 = y_0 - y_1, \quad (15)$$

we obtain

$$Q(u, v) = 2|A(u, v)|\exp[j\phi(u, v)] \times \exp\{-j2\pi[u(x_1 + x_2) + v(y_1 + y_2)]\}\cos[2\pi(ux_2 + vy_2)], \quad (16)$$

leading to

$$G'(u, v) = N_{l=0}\{Q(u, v)\}P'(u, v) = \exp\{-j2\pi[u(x_1 + x_2) + v(y_1 + y_2)]\}\mathrm{sgn}\{\cos[2\pi(ux_2 + vy_2)]\}. \quad (17)$$

By employing the Fourier series expansion

$$\mathrm{sgn}\{\cos[2\pi(ux_2 + vy_2)]\} = \frac{4}{\pi}\sum_{k=1}^{\infty} a_k \cos[[2k - 1][2\pi(ux_2 + vy_2)]], \quad (18)$$

where $a_k = (-1)^{k-1}/(2k-1)$, after substitution of Eq. (18) into Eq. (17) and with Eq. (7) we obtain

$$C(x,y) = \frac{2}{\pi}\{\delta[x+(x_1+2x_2)]\delta[y+(y_1+2y_2)] + \delta(x+x_1)\delta(y+y_1) + \sum_{k=2}^{\infty} a_k[\delta[x-x_1-x_2-(2k-1)x_2]\delta[y-y_1-y_2-(2k-1)y_2] + \delta[x-x_1-x_2+(2k-1)x_2]\delta[y-y_1-y_2+(2k-1)y_2]]\}. \quad (19)$$

After returning to the original parameters [Eq. (15)] we obtain

$$C(x,y) = \frac{2}{\pi}\{\delta(x+x_0)\delta(y+y_0) + \delta(x+x_1)\delta(y+y_1) + \sum_{k=2}^{\infty} a_k[\delta[x-x_1-x_2-(2k-1)x_2]\delta[y-y_1-y_2-(2k-1)y_2] + \delta[x-x_1-x_2+(2k-1)x_2]\delta[y-y_1-y_2+(2k-1)y_2]]\}. \quad (20)$$

Since we can measure only the intensity distribution in the correlation plane and since the square of the sum of spatially separated delta functions is equal to the sum of their squares, we obtain the intensity distribution in the correlation plane in the form

$$I_C(x,y) \propto \delta(x+x_0)\delta(y+y_0) + \delta(x+x_1)\delta(y+y_1) + \sum_{k=2}^{\infty} a_k^2[\delta[x-x_1-x_2-(2k-1)x_2]\delta[y-y_1-y_2-(2k-1)y_2] + \delta[x-x_1-x_2+(2k-1)x_2]\delta[y-y_1-y_2+(2k-1)y_2]]. \quad (21)$$

The various diffraction orders in relation (21) are attenuated as a_k^2. Having $a_2^2 = 1/9$, $a_3^2 = 1/25$, and the general term $a_n^2 = (2n-1)^{-2}$, we observe that the side peaks are quite low in magnitude. A typical plot of relation (21) that is shown in Fig. 2 indicated that only the first order, where the true correlation term appears, contains considerable energy.

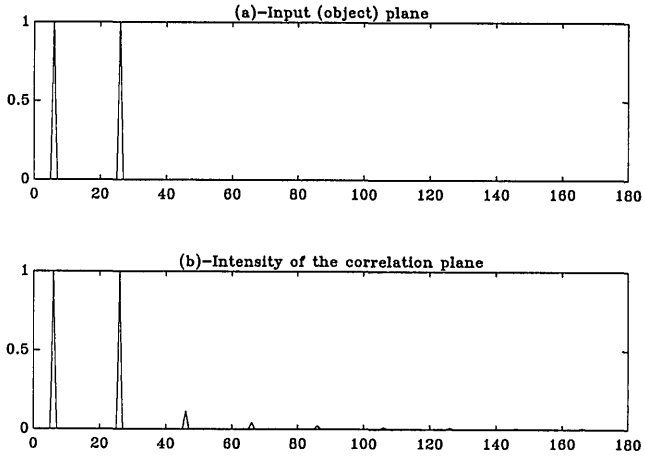

Fig. 2. (a) Input distribution; (b) intensity distribution over the correlation plane.

III. Multiple Input Interference Effects

The examples of Section II indicate that some difficulties may arise when more than a single object is present in the input plane. Similar difficulties were observed in the nonlinear binary JTC.[9,10] For a complicated input scene the real amplitude distribution of its FT contains information about the separate objects as well as the linear phases determined by their relative positions. Thus, vital information regarding these positions may be lost by ignoring the intensity distribution. The following example illustrates this point. Assume a pattern of four point sources in the input (spatial delta functions), equally spaced at $-3x_0$, $-x_0$, x_0, $3x_0$. The FT of the input, $q(x)$, yields a sum of linear phases (for simplicity a one-dimensional signal is assumed):

$$q(x) = \sum_{n=1}^{4} \delta[x-(2n-5)x_0], \quad (22)$$

$$\mathcal{F}\{q(x)\} = \sum_{i=1}^{4} \exp(jx_i 2\pi u) = \frac{\sin(8\pi u x_0)}{\sin(2\pi u x_0)}. \quad (23)$$

In the limit, when we have an infinite number of point sources equally spaced, $|\mathcal{F}\{q(x)\}|$ turns into a train of delta functions. Consequently, the amplitude distribution is of utmost importance. Thus we see that the phase information (the linear phases) that contains the information concerning the location of the objects in the input is coded into the amplitude distribution as well. Hence, ignoring the amplitude distribution may generate false correlation peaks or suppress existing correlation peaks.

The above effect was observed in computer simulations whenever identical input objects were arranged in a line at regular intervals. However, when the objects were arranged randomly, the information regarding the positions of the objects were preserved in the phase distribution and true correlation peaks were obtained at the correct positions.

To conclude this topic it may be stated that manipulation of only the phase information should generate narrow correlation responses with no false peaks so long as the amplitude distribution of the pattern is not, to a large extent, modulated by the linear phase due to the location of the individual patterns. Otherwise the location information is coded into the amplitude distribution as well (which is ignored) and, consequently, a distorted correlation output may result.

The above-described interference problem may be alleviated by introducing an adaptive threshold of the form

$$N_t[R(u,v)] = \begin{cases} \exp[j\varphi_R(u,v)] & \text{if } |R(u,v)| \geq t(u,v), \\ 0 & \text{otherwise,} \end{cases} \quad (24)$$

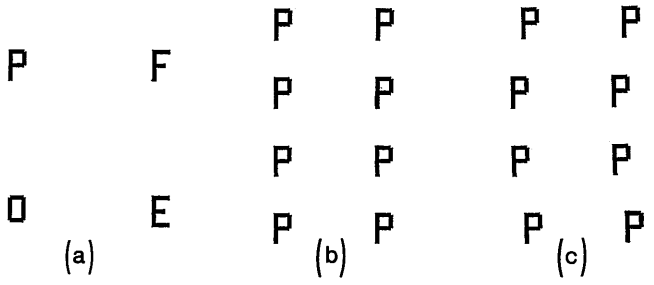

Fig. 3. Three input distributions used in the simulations.

where $t(u, v)$ is a spatially varying threshold. For example,

$$t(u, v) = \mu \frac{|\mathcal{F}\{p(x, y)\}|}{\max[|\mathcal{F}\{p(x, y)\}|]}, \quad 0 \le \mu < 1. \tag{25}$$

Clearly, Eq. (24) presents a selective mapping of the complex domain to the complex domain. All the vectors that are greater than or equal to $t(u, v)$ are mapped to the unit circle and to zero otherwise. This is to be contrasted with Eq. (1) in which the original nonlinear mapping, with $l = 0$, is described, in which all vectors to the unit circle are mapped. By choosing the above adaptive threshold, we may achieve an output that is totally independent of the specific input function. This is so since for a single input object, to which the filter is matched, the ideal output correlation is always a delta function of the same energy located at the object's center. Even for the case of several similar objects in the input plane, the correlation peaks are largely independent of the specific arrangement of the objects in the input plane. The above choice of threshold function, given by Eq. (25), guarantees that we follow the envelope of $\mathcal{F}\{p(x, y)\}$ to which the filter is matched. Hence low-amplitude, noisy information of the subsidiary maxima generated by the sum of the linear phases that would degrade performance is not amplified. This approach is similar to the methods that have improved the POF and binary POF[12] and motivated the development of the ternary phase amplitude filter.[13]

The FT of N identical objects with the one-dimensional distribution $a(x)$, equally spaced with displacement $2x_0$, symmetrically placed with respect to the origin, is

$$\mathcal{F}\left\{\sum_{n=-\frac{N}{2}}^{\frac{N}{2}} a(x - 2nx_0)\right\} = A(u) \frac{\sin(2\pi N x_0 u)}{\sin(2\pi x_0 u)}. \tag{26}$$

When the adaptive threshold, as given in Eqs. (24) and (25), is performed and the result is multiplied by the proper POF, we obtain the distribution

$$\sum_{n=-\infty}^{\infty} \mathrm{rect}\left(\frac{u - \frac{n}{2x_0}}{a}\right), \tag{27}$$

where a is calculated by the relation

$$\frac{\sin(\pi N x_0 a)}{\sin(\pi x_0 a)} = \mu N. \tag{28}$$

The FT of expression (27) yields a correlation plane distribution of the form

$$\sum_{n=-\infty}^{\infty} \delta(x - 2nx_0)\mathrm{sinc}\left(\frac{ax}{\pi}\right). \tag{29}$$

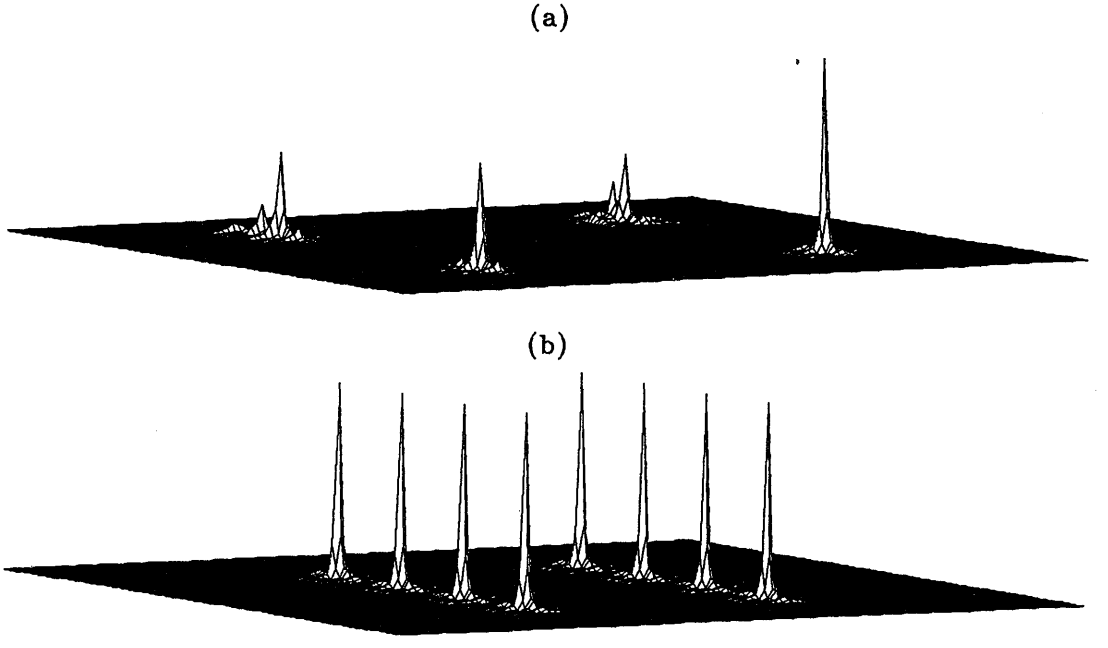

Fig. 4. Correlation plane with a POF, matched to P, produced by a linear correlator: (a) Fig. 3(a) as the input, (b) Fig. 3(b) as the input.

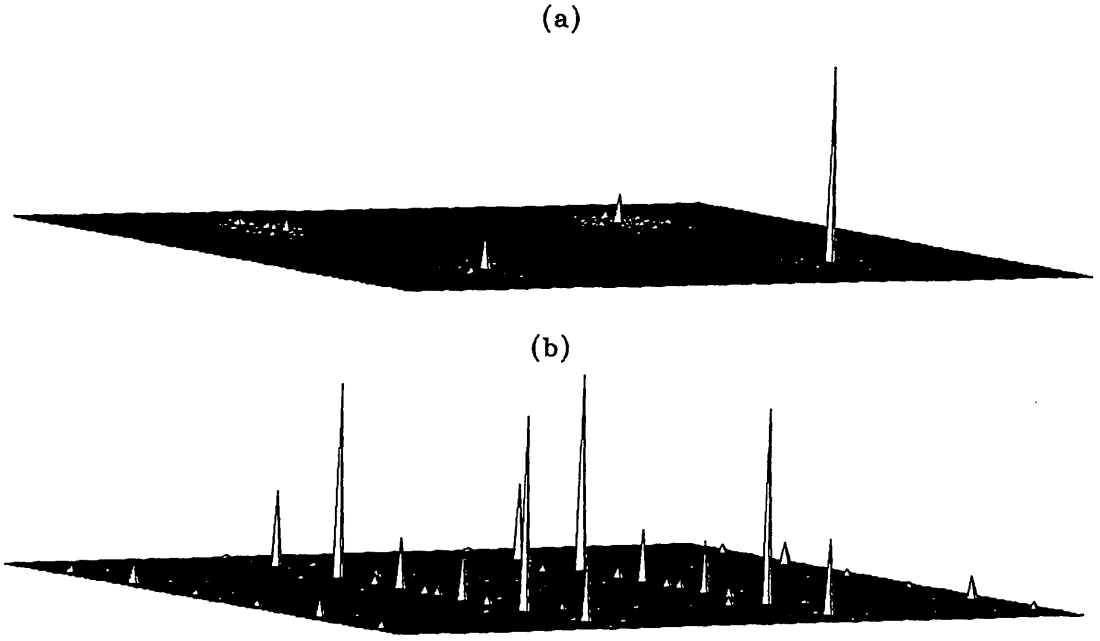

Fig. 5. Same as Fig. 4 but with the phase extraction correlator.

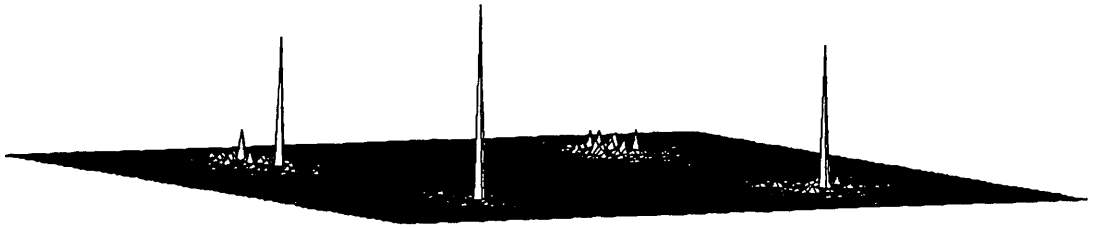

Fig. 6. Same as Fig. 5(a) but with F as the filter function.

IV. Computer Simulations

Letters of size 10 × 10 pixels were generated and placed in an input plane of size 128 × 128 pixels. The FT of the input was taken when a fast Fourier transform was used. The POF was also stored in 128 × 128 pixels. Finally, the correlation plane was obtained by taking the FT of the product of the POF and the result of the nonlinearity applied to the FT of the input.

Various inputs used in the simulations are shown in Fig. 3. The correlations obtained with a conventional linear correlator employing a POF matched to the letter P are shown in Fig. 4. The correlation plane shown emulates exactly the correlation performed optically with two consecutive FT's (not a FT followed by an IFT). The correlations obtained with the phase extraction correlator described by Eqs. (2)–(7) with the filter matched to the letter P are shown in Fig. 5 and with the filter matched to F are shown in Fig. 6. Note that the discrimination against the letters E and P when F is used as the filter is poor since, in our choice of the letters E and P, both contain the letter F. Various metrics relating to Figs. 4(a) and 5(a) are grouped in Table I and compared with the conventional POF. Peak-to-correlation energy (PCE) in the table is a parameter measuring the sharpness of the peak.[14]

Table I. Normalized Merit Factors[a]

Various Metrics	Linear Correlator with POF	NL Correlator with POF
Rejection	1.82	5.56
PCE	0.333	1

[a]Derived from the simulation results given by Figs. 4(a) and 5(a) where rejection = peak corresponding to P/peak corresponding to F; PCE = correlation peak intensity/$\int_{-\infty}^{\infty}\int_{-\infty}^{\infty}|C(x,y)|^2 dxdy$.

Table II. Correlation Response (in Arbitrary Units) at $\pm x_0$, $\pm bx_0$ to Four Identical Objects Centered at $-bx_0$, $-x_0$, x_0, bx_0 with the Phase Extraction Pattern Recognition System[a]

b	=2	=3	=4	=10
Correlation				
$\|C_b(\pm x_0)\|$	1.36	0.65	1.057	1.0083
$\|C_b(\pm bx_0)\|$	0.68	1.26	0.944	0.992
$\|C_b(bx_0)/C_b(x_0)\|^2$	0.25	3.75	0.89	0.99

[a]$C_b(x_0)$ is the correlation response C at x_0 when b is as given in the table. $C_b(bx_0)$ is the correlation response C at bx_0 when b is as given in the table.

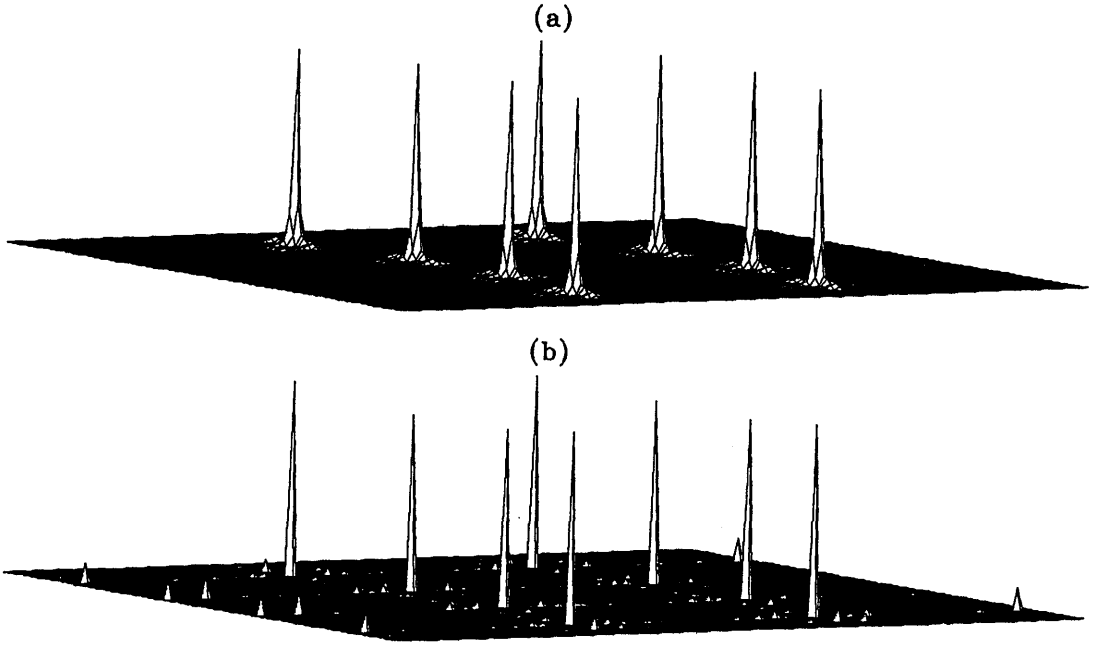

Fig. 7. Figure 3(c) as the input for correlation with P: (a) conventional POF, (b) phase extraction correlator.

As we mentioned in Section III, when the objects are arranged in some orderly pattern the NL correlator does not perform well. A careful analytical examination of the height of the correlation peaks generated by the phase extraction correlator, for the identical four-object case, as a function of displacement, produced the results presented in Table II. The ratio between the true correlation peaks, $|C_b(bx_0)/C_b(x_0)|^2$, varies erratically the closer the objects' arrangement is to mimic a pattern. As the objects' arrangement leaves the pattern arrangement (in Table II this corresponds to $b = 3$ and to a smaller degree $b = 2$) toward a disordered arrangement ($b = 4$, 10), the true correlation peaks settle down to a similar value, i.e., the ratio $|C_b(bx_0)/C_b(x_0)|^2$ is ~ 1.

Consider the case shown in Fig. 3(b) (four equally spaced identical objects arranged in two lines, which would correspond to $b = 3$ in Table II). The corresponding output correlation planes are shown in Fig. 4(b) for the linear POF and in Fig. 5(b) for the phase extraction correlator. It is evident from Fig. 5(b) that the heights of the peaks at the true positions of the objects are not of the same height. Moreover, spurious peaks are generated whose height exceeds the height of the true position peaks. This problem is not encountered when the letters are arranged in a disordered manner as in Fig. 3(c). The correlation response for this case is good as is obvious from Fig. 7(b). The variation in the intensity of the true peak heights is $< 10\%$ and the false peak heights are small.

Figure 8 shows a typical result obtained with a NL adaptive correlator when the threshold of Eq. (25) was used. Although the problem of true peak variance is not completely solved, it is dramatically mitigated since the subsidiary peaks (false position peaks) have been drastically suppressed such that the largest subsidiary false peak is $< 25\%$ of the minimal true location peak. This may be clearly seen in Fig. 8.

V. Electro-Optical Architecture

The electro-optical system that implemented the idea of Fig. 1 is shown in Fig. 9. Note that this architecture closely follows Eqs. (2)–(7) that describe Fig. 1. The operation is as follows:

A transparency containing the filter function $p(x,y)$ is placed at the input plane in the lower channel of Fig. 9. Lens L_1 of focal length f performs a FT to the camera plane. Subsequently it is superposed with a plane wave of amplitude A and at an angle θ. The

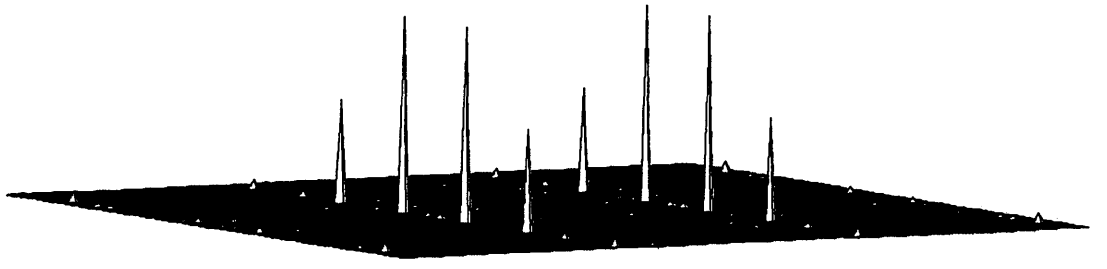

Fig. 8. Output correlation plane with an adaptive NL correlator with Fig. 3(b) as the input.

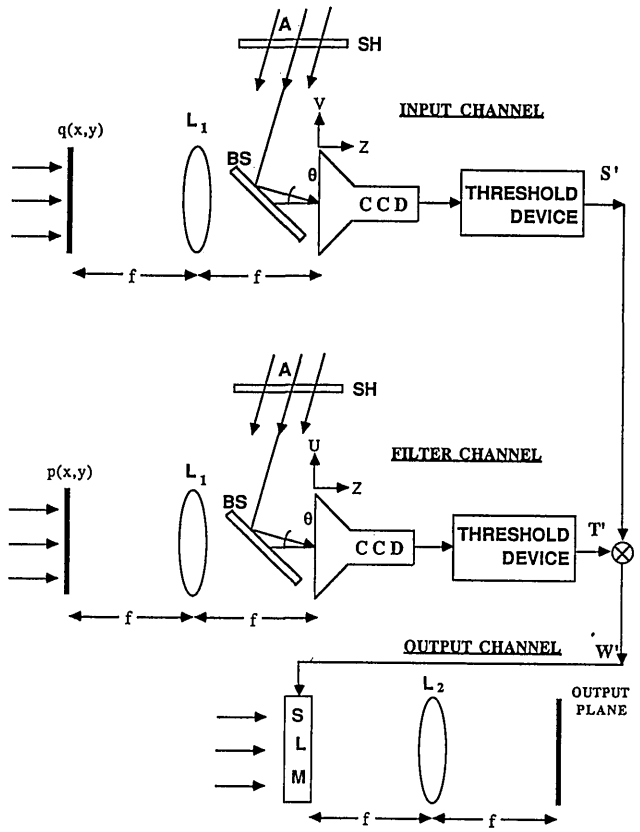

Fig. 9. Electro-optical implementation of Fig. 1.

angle is set such that the wave vector is parallel to the u–z plane.

The interference pattern recorded by the camera is given by

$$T(u, v) = |A|^2 + |P(u, v)|^2 + 2|A||P(u, v)| \cos[2\pi\alpha u + \Phi_P(u, v)], \quad (30)$$

where

$$\alpha = \frac{\sin(\theta)}{\lambda}, \quad (31)$$

$$\Phi_P(u, v) = \arg[P(u, v)]. \quad (32)$$

The intensity distribution of $P(u, v)$ is also recorded separately for the subsequent thresholding by closing shutter SH in Fig. 9. A thresholding operation,

$$T'(u, v) = \begin{cases} -1 \text{ if } T(u, v) < |A|^2 + |P(u, v)|^2 \\ 1 \text{ otherwise} \end{cases}, \quad (33)$$

is performed by the computer. This thresholding operation can also be written as

$$T'(u, v) = \operatorname{sgn}[\cos[2\pi\alpha u + \Phi_P(u, v)]] \quad (34)$$

or, in a series expansion, as

$$T'(u, v) = \sum_{n=-\infty, n \text{ odd}}^{\infty} \frac{2}{n\pi}(-1)^{\frac{(n-1)}{2}} \exp[jn[2\pi\alpha u + \Phi_P(u, v)]]. \quad (35)$$

The FT of Eq. (35) yields an infinite number of diffraction orders (harmonics) along the x axis. The first orders, centered at $(\pm\lambda f\alpha, 0)$, correspond to the FT of $\exp[\pm j\Phi_P(u, v)]$, respectively, as shown in Fig. 10(a). This completes the preparation stage—the learning process.

To operate the system for its pattern recognition task after the learning procedure is completed, a

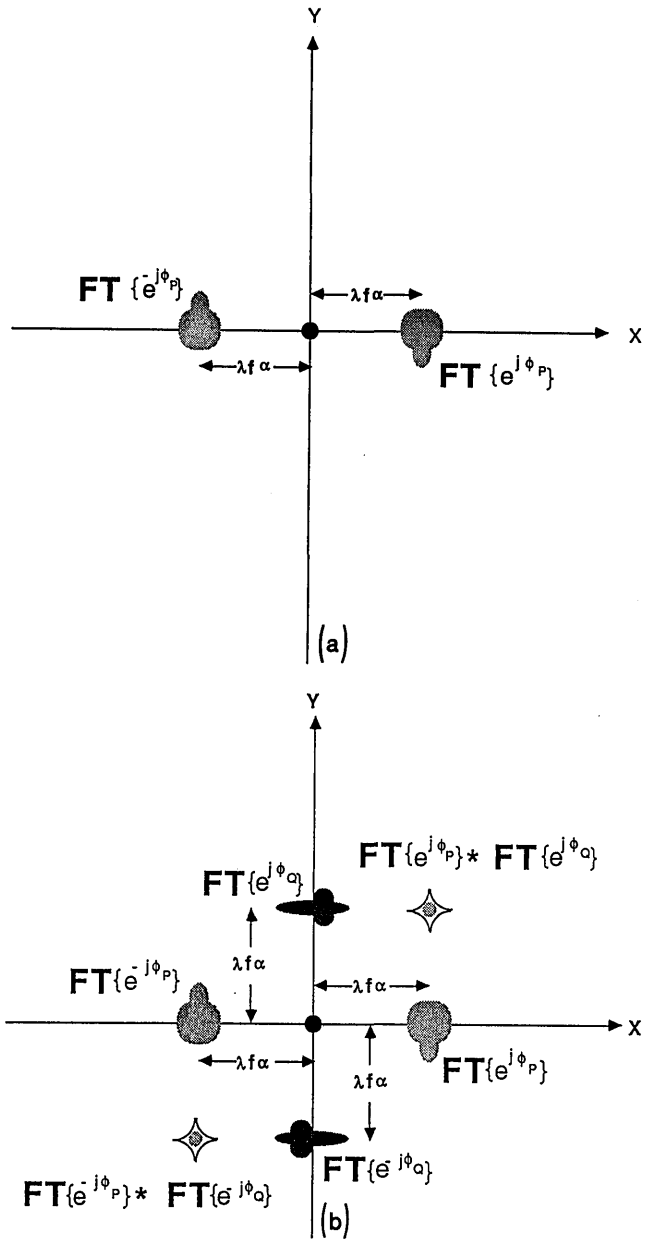

Fig. 10. (a) The FT of $T'(u, v)$. (b) FT of $W'(u, v)$, the output correlation plane. The orders where the desired correlations were obtained are marked.

similar process is repeated for the input function $q(x, y)$. This is implemented in the upper channel of Fig. 9 except for the fact that the angle of the plane wave is altered such that the wave vector is parallel to the v–z plane, i.e., perpendicular to the wave vector that was used to generate the filter. Hence we obtain

$$S'(u, v) = \operatorname{sgn}\{\cos[2\pi\alpha v + \Phi_Q(u, v)]\}. \tag{36}$$

Again, Eq. (36) may be rewritten as

$$S'(u, v) = \sum_{n=-\infty, n \text{ odd}}^{\infty} \frac{2}{n\pi}(-1)^{\frac{(n-1)}{2}} \exp[jn[2\pi\alpha v + \Phi_Q(u, v)]]. \tag{37}$$

The FT of Eq. (37) yields an infinite number of diffraction orders (harmonics) along the y axis. The first orders, centered at $(0, \pm \lambda f\alpha)$, correspond to the FT of $\exp[\pm j\Phi_G(u, v)]$, respectively.

After multiplying $S'(u, v)$ by $T'(u, v)$ we obtain $W'(u, v)$, which is displayed on the spatial light modulator. $W'(u, v)$, which is a bipolar grating, is written on the magneto-optic spatial light modulator in a method proposed by Psaltis *et al.*[15] The desired cross correlation is obtained, after performing an optical FT, either at the order (1, 1) or at the order $(-1, -1)$. The only relevant terms from $W'(u, v)$ are

$$\frac{4}{\pi^2} \exp\{-j[2\pi\alpha u + 2\pi\alpha v + \Phi_P(u, v) + \Phi_Q(u, v)]\}$$

or

$$\frac{4}{\pi^2} \exp\{+j[2\pi\alpha u + 2\pi\alpha v + \Phi_P(u, v) + \Phi_Q(u, v)]\}$$

and their FT results in the cross correlation. This is shown in Fig. 10(b).

The actual experiment in the laboratory was performed in a single optical channel (Fig. 11) in three time cycles. To obtain the two different wave vectors of the plane wave the mirror was properly tilted for the learning and recognition cycles.

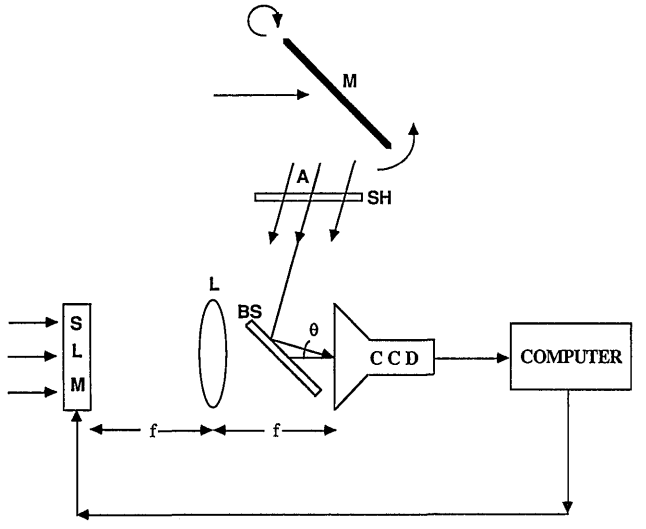

Fig. 11. The $2f$ laboratory setup executing the same process as in Fig. 9 in three cycles.

VI. Laboratory Experiments

When the electro-optical system described in Section 5 was used several experiments were performed. The system was controlled by an IBM AT-compatible computer supplemented with a CUE-2 package.[16]

In one of the experiments a filter was prepared to match the letter P. The binarized interference pattern of the filter, $T'(u, v)$ [Eq. (35)], is shown in Fig. 12(a). The binarized interference pattern of the input (also a single letter P), $S'(u, v)$, which is given by Eq. (37), is shown in Fig. 12(b). Note that the fringes in Fig. 12(b) are perpendicular to those of Fig. 12(a), as required. The product of $S'(u, v)$ and $T'(u, v)$, $W'(u, v)$, is given in Fig. 12(c). The transverse cross section of the correlation peak, obtained by a FT of Fig. 12(c), is given in Fig. 12(d).

By using the same filter but with the input of Fig. 3(a) we obtained a W' as shown in Fig. 13(a). The FT of W' is shown in Fig. 13(b). In both Figs. 13 and 14 the correlation areas [which is the region of the (1, 1) order of Fig. 10(b)] are surrounded by a white square. A strong peak at the position of the correlation with the letter P is clearly observed while the letters F, O, and E are dramatically rejected, as required. This is made even clearer in Fig. 13(c) where a cross section of the relevant correlation peaks of P and F is shown. Note the excellent agreement with the simulation results [Fig. 5(a)].

Finally, by using the same input as for Fig. 13, we generated $W'(u, v)$ with the filter matched to F; this is shown in Fig. 14(a). The FT of W' is shown in Fig. 14(b). We observe strong peaks at the positions that correspond to the letters P, F, and E as predicted in the simulations (Fig. 6).

We also investigated the performance of the correlator when the input to the system is an orderly pattern of equally spaced objects as shown in Fig. 4(b). In this case, as shown above, we expect the true peaks not to be of the same height (as shown in Table II) and false correlation peaks to be generated that are higher than the true correlation peaks [see Fig. 5(b)]. Not withstanding this, in the laboratory, the correlator performed well for this case, i.e., it recognized all eight P's present in the input at the correct positions and with low sidelobes. This is clearly shown in Fig. 15(a). Note that the peaks are approximately of the same height, as is clearly demonstrated in Fig. 15(b). The reason for this appears to be the noise and aberrations present in the actual optical system that corrupts the ordering. Hence the magnitude of the false peaks observed in the ideal simulations is substantially reduced.

VII. Efficiency Considerations

One interesting and useful attribute of the phase extraction correlator is that the output correlation peak is independent of the particular input function. For a single object input to which the filter is matched

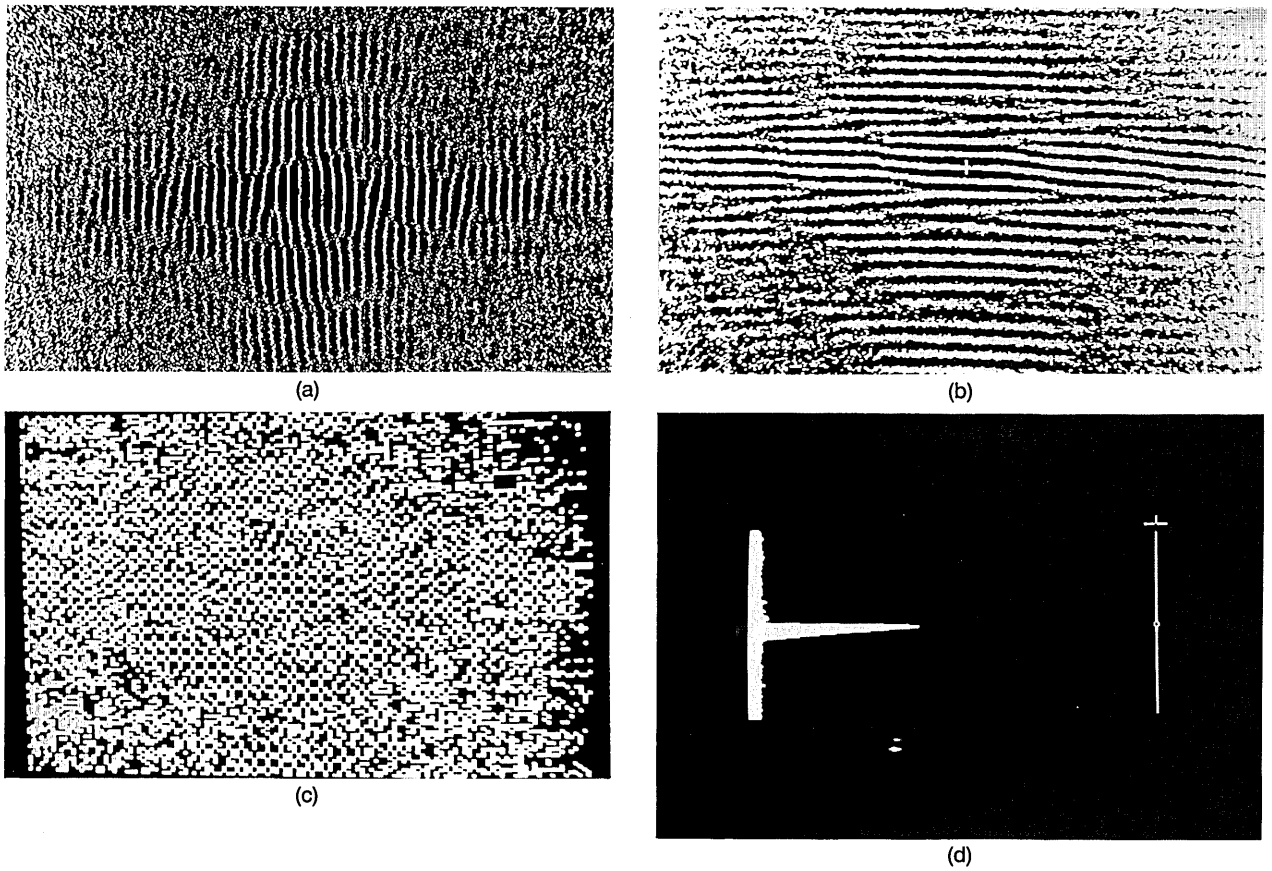

Fig. 12. (a) Binarized interference pattern of the POF matched to the letter P, $T'(u, v)$. (b) Binarized interference pattern of the input (also a single letter P) $S'(u, v)$. (c) W', the product of S' and T'. (d) FT of W' with the transverse cross section of the (1, 1) correlation peak.

the output correlation peak is always a delta function having the same energy. By defining the optical efficiency as the ratio between the integrated intensity of the (1, 1) order (correlation spot) and the integrated intensity in the correlation plane (distributed in all the diffraction orders), we achieve, theoretically, the efficiency

$$\eta = \frac{\left(\frac{s}{\pi}\right)^4}{\sum_{n=-\infty}^{\infty}\sum_{m=-\infty}^{\infty}{}_{m,n\in\text{odd}}\left|\frac{2}{n\pi}\frac{2}{m\pi}\right|^2} = (1.03 \times s^4)\%,$$

where

$$s = \begin{cases} 2 \text{ if the thresholding operation results are} \\ \quad \text{bipolar (1 and } -1\text{) as in this paper,} \\ 1 \text{ if the thresholding operation results are} \\ \quad \text{unipolar (1 and 0).} \end{cases} \tag{38}$$

It is clear that the efficiency of the bipolar phase extraction correlator is much higher than the unipolar phase extraction correlator that we presented elsewhere.[17]

Remembering that the correlation peak with a single object as an input is located at one single point (δ-function output) means that the effective efficiency of the proposed correlator is even higher compared to other conventional correlators. This efficiency is also compared to the efficiency of an inverse filter in a linear system. Although the efficiency of a linear inverse filter is function dependent, we may still evaluate it by using the evaluation of Horner[11] based on typical objects and dimensions. According to the results of Horner the efficiency of the linear correlator is 0.01% with a direct, nongrating filter when an inverse filter is used. When taking into account that we need a binary computer-generated hologram for the filter implementation means that the efficiency is further reduced by another order of magnitude since the efficiency of computer-generated holograms is $< 10\%$.[18] By comparing this to the efficiency of 16% of our bipolar correlator [$s = 2$ in Eq. (38)] we see that the improvement in the optical efficiency put forward by our NL system is dramatic. It should, however, be noted that the 16% efficiency is a theoretical efficiency if we assume that a uniform grating is generated in the frequency plane. This is not practical because of the noise present in the system as is obvious from Figs. 12–14.

It should also be noted that the output correlation plane is illumination invariant, i.e., independent of illumination on the object. It is also evident that the

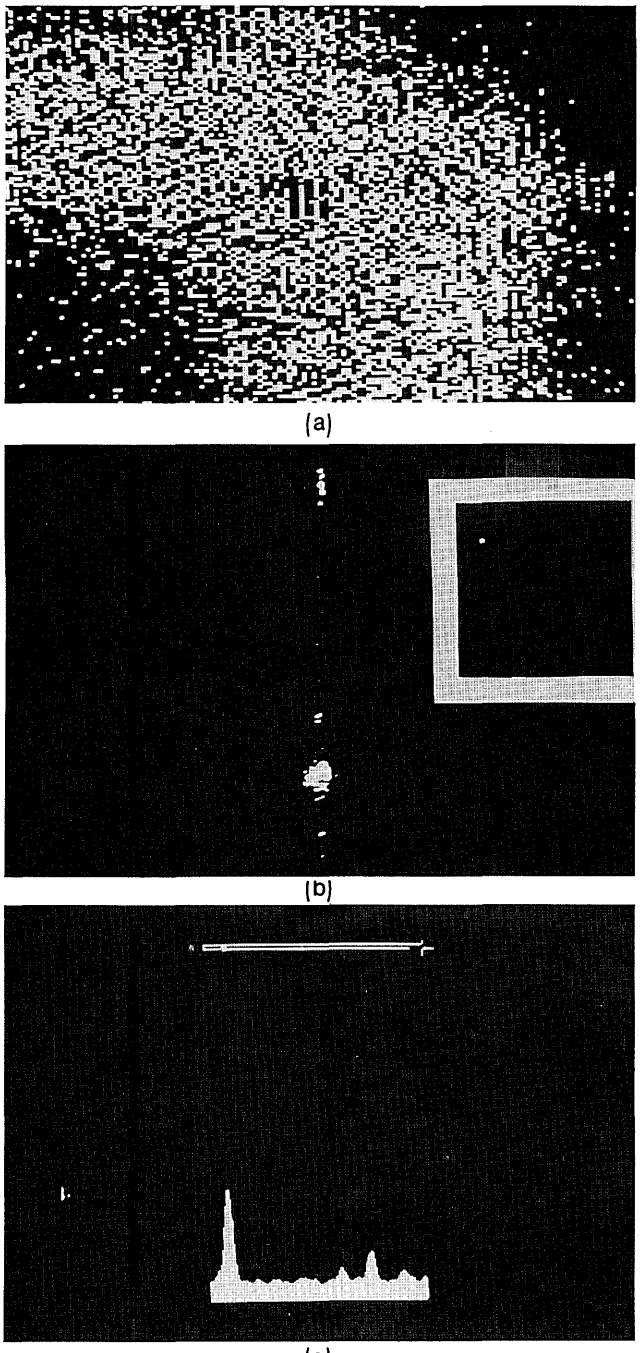

Fig. 13. (a) W' with Fig. 3(a) as the input and P as the filter. (b) The FT of W' (the dimensions of the added white border are approximately the size of the input plane). (c) Cross section of the section corresponding to the letters P and F in (b).

system is shift invariant in that shifting the input plane, as a whole, will cause a corresponding shift in the output correlation plane. However, as in the JTC, the height of the correlation peaks is dependent on the number of objects in the input.

VIII. Architectural Modifications

The phase extraction correlation system is shown diagrammatically in Fig. 1. It should however be

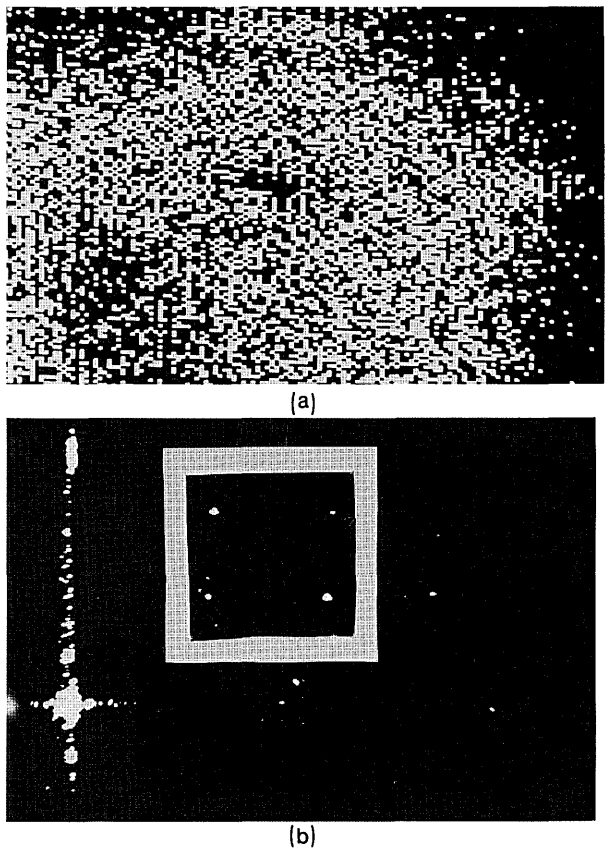

Fig. 14. As in Fig. 13 but with F as the filter.

appreciated that, because of the symmetry of the system and the type of nonlinearity employed as given by Eq. (1), we may simplify Fig. 1 to Fig. 16. This is so since

$$N_i[Q(u,v)] = Q'(u,v) = |Q(u,v)|^l \exp[j\varphi_Q(u,v)];$$
$$N_i[P(u,v)] = P'(u,v) = |P(u,v)|^l \exp[j\varphi_P(u,v)]; \quad (39)$$

therefore

$$N_i[Q(u,v)]N_i[P(u,v)] = N_i[Q(u,v)P(u,v)]. \quad (40)$$

Hence the output correlation plane of Fig. 1 is identical to that of Fig. 16 if the same input and filter functions are used for both figures.

Also, we are not confined to use a specific filter for multiplication by the FT of the input. In fact we may use any filter (having any amplitude and phase distribution). Thus, the NL operation may be performed prior or subsequent to the actual multiplication in the frequency domain, i.e., we may perform pre- or post-NL processing in our system without alteration of the results. As a matter of fact the NL operations may be performed on correlation results obtained from a linear system if the amplitude and phase distribution of the output of the linear correlation system are available. In other words, a true postprocessing system may be realized without any degradation in system performance.

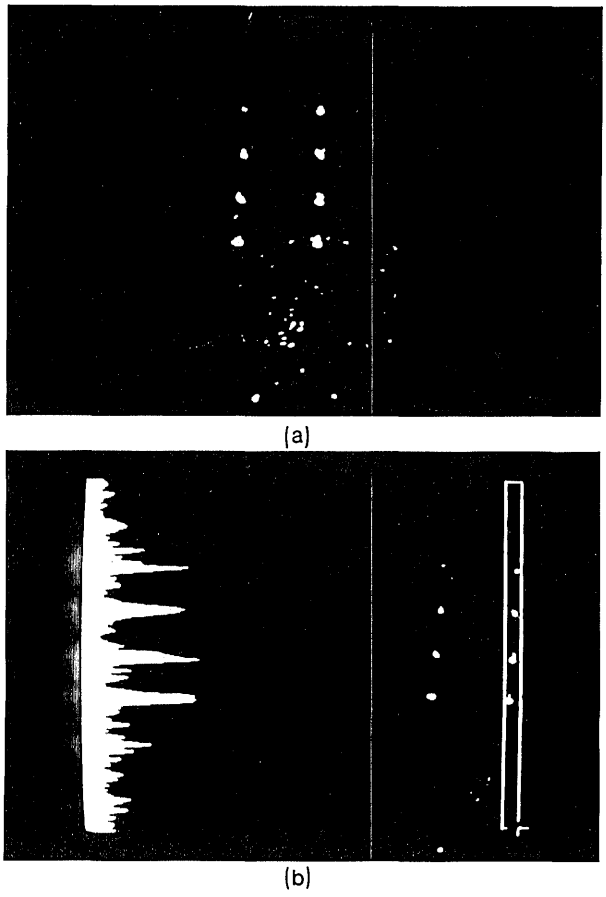

Fig. 15. (a) FT of W' obtained with Fig. 3(b) as the input and P as the filter. (b) Cross section of (a).

IX. Conclusions

We have demonstrated the feasibility of achieving electro-optical phase extraction pattern recognition and have observed the various advantages of such a system. Although the system is somewhat more complex than a linear correlator, the hybrid system is not difficult to build. Also, since both the input and the filter are processed in quasi-real time and in the same optical system, the optical distortions are accounted for. Moreover, as all our inputs are binary (± 1), the input may also be displayed on a binary spatial light modulator. Hence it may be possible to convert the $4f$ correlator to a compact $2f$ correlator. Despite bearing some problematic features, the worst of which is probably the sensitivity to a periodic arrangement of patterns, the phase extraction correlator demonstrated considerable success. As presented, the problematic features may be alleviated, if not totally mitigated, by suitable adaptation algorithms that are currently under further investigation.

In summary, we have demonstrated a phase extraction correlator with inverse filterlike performance, i.e.,

High discrimination: Supported by Table I and simulations given in Section IV. Also it should be appreciated that because of the NL operation the high spectral frequencies are amplified. Since the differences between objects lie in the high frequencies, in general, we expected the phase extraction correlator to give good discrimination because of its intrinsic amplification attribute.

Sharp correlation peaks: We showed that for object(s) to which the filter is matched [see Eqs. (10) and (20)] the correlation peaks are delta functions—the sharpest possible functions.

High energy transfer: Clearly, from Eq. (38) the energy transfer is very high (16% for $s = 2$) compared with that of other correlators having the same peak sharpness, e.g., the inverse filter. This means that we should be able to use a low-powered laser in such a correlation system.

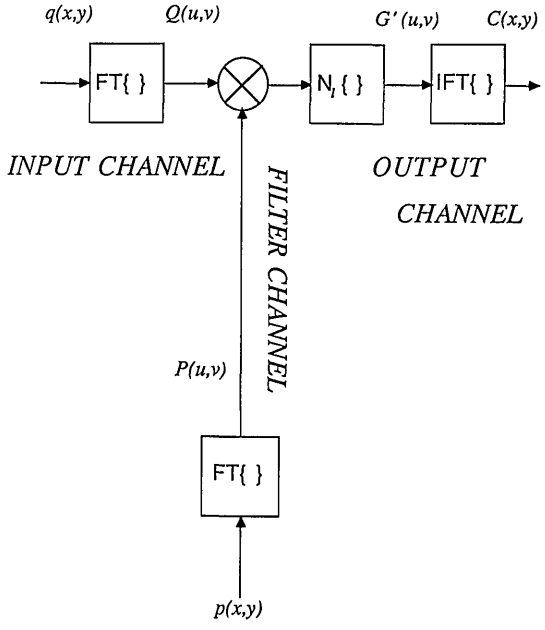

Fig. 16. Alternative realization of the NL correlator of Fig. 1.

This work was performed within the Technion Advanced Opto-Electronics Center established by the American Technion Society, New York.

References

1. A. VanderLugt, "Signal detection by complex spatial filtering," IEEE Trans. Inf. Theory **IT-10,** 130–145 (1969).
2. A. V. Oppenheim and J. S. Lim, "The importance of phase in signals," Proc. IEEE **69,** 529–541 (1981).
3. J. L. Horner and P. D. Gianino, "Phase-only matched filtering," Appl. Opt. **23,** 812–816 (1984).
4. T. Nomura, K. Itoh, K. Matsuoka, and Y. Ichioka, "Binary Fourier phase-only correlation," Opt. Lett. **15,** 810–811 (1990).
5. O. K. Ersoy and M. Zeng, "Nonlinear matched filtering," J. Opt. Soc. Am. A **6,** 636–648 (1989).
6. O. K. Ersoy, Y. Yoon, N. Keshava, and D. Zimmerman, "Nonlinear matched filtering," Opt. Eng. **29,** 1002–1012 (1990).
7. B. Javidi, C. J. Kuo, and S. F. Odeh, "Comparison of bipolar joint transform image correlators and phase only matched filter correlator," in *Digital and Optical Shape Representation and Pattern Recognition,* R. D. Juday, ed., Proc. Soc. Photo-Opt. Instrum. Eng. **938,** 66–75 (1988).

8. B. Javidi and J. Wang, "Binary nonlinear joint transform correlation with median and subset thresholding," Appl. Opt. **30,** 967–976 (1991).
9. F. T. S. Yu, F. Cheng, T. Nagata, and D. A. Gregory, "Effects of fringe binarization of multiobject joint transform correlation," Appl. Opt. **28,** 2988–2990 (1989).
10. W. Hahn and D. Flannery, "Basic design elements of binary joint-transform correlation and selected optimization techniques." in *Optical Information Processing Systems and Architectures II,* B. Javidi, ed., Proc. Soc. Photo-Opt. Instrum. Eng. **1347,** 344–356 (1990).
11. J. L. Horner, "Light utilization in optical correlators," Appl. Opt. **21,** 4511–4514 (1982).
12. B. Kumar and Z. Bahri, "Efficient algorithm for designing a ternary valued filter yielding maximum signal-to-noise ratio," Appl. Opt. **28,** 1919–1925 (1989).
13. D. L. Flannery, J. S. Loomis, and M. E. Milkovich, "Transform-ratio ternary phase-amplitude filter formulation for improved correlation discrimination," Appl. Opt. **27,** 4079–4083 (1988).
14. B. V. K. Vijaya Kumar, W. Shi, and C. Hendrix, "Phase-only filters with maximally sharp correlation peaks," Opt. Lett. **15,** 807–809 (1990).
15. D. Psaltis, E. G. Paek, and S. S. Venkatesh, "Optical image correlation with a binary spatial light modulator," Opt. Eng. **23,** 698–704 (1984).
16. The CUE-2 is an image processing system based on a personal computer manufactured by Galai Laboratories, Industrial Zone, Migdal Haemek, Israel.
17. T. Kotzer, J. Rosen, and J. Shamir, "Phase extraction pattern recognition," in *Optical Society of America 1990 Annual Meeting,* Vol. 15 of OSA 1990 Technical Digest Series (Optical Society of America, Washington, D.C., 1990), p. 225.
18. B. R. Brown and A. W. Lohmann, "Computer-generated binary holograms," IBM J. Res. Dev. **13,** 160–168 (1969).